Earth and Planetary Science Letters 272 (2008) 709–719

Contents lists available at ScienceDirect

Earth and Planetary Science Letters

journal homepage: www.elsevier.com/locate/epsl

Influence of major inherited faults zones on gravitational slope deformation: A two-dimensional physical modelling of the La Clapière area (Southern French Alps)

T. Bois *, S. Bouissou, Y. Guglielmi

Géosciences Azur, UMR 6526, Université de Nice Sophia-Antipolis, Valbonne, France

ARTICLE INFO

Article history:
Received 12 February 2008
Received in revised form 23 May 2008
Accepted 4 June 2008
Available online 18 June 2008

Editor: L. Stixrude

Keywords:
Deep-Seated Gravitational Deformation
sackungen
sackung
deep-seated failure
landslide
La Clapière
structural heterogeneities
listric faults
thrust fault
physical modelling

ABSTRACT

Inherited faults are known to influence rock slope stability and gravitational deformation. In spite of that, in many studies few faults are identified in field and properly used in models of gravitational slope deformation. The aim of this work is to study the influence of inherited faults zone density and geometry on gravitational failure processes at the massif scale using a physical modelling technique which satisfies the similarity criteria. Models are scaled to the well-documented natural example of La Clapière in the Southern French Alps. Experiments were conducted using mechanically homogeneous material with variable fault geometry. In each of tested configurations, the mobilized volume was almost the same. Results confirmed the hypothesis that the La Clapière landslide is a shallow section of a deep-seated gravitational slope deformation. Furthermore, among the various configurations tested, only one is enable to reproduce the observed superficial deformation on the La Clapière hillside. This result demonstrated that the geometry of the faults at depth plays a major role on the style of gravitational deformation patterns. Regarding the particular case of La Clapière, our results give new insights on the shape of the faults affecting the massif at depth. In particular, normal listric faults seem to have shallow inflexions compared to a deep-seated thrust fault that was either gravitationally formed or pre-existing but inactive (i.e. sealed) before slope destabilization and then gravitationally reactivated.

1. Introduction

Gravitational Slope Deformations are common in all mountain ranges (Crosta, 1996; Agliardia et al., 2001, Tibaldi et al., 2004). They can be very slow deformations, also called “Sagging” or “Sackung”, characterized by morpho-structural features such as double ridges, ridge top depressions, scarps and counterscarps, trenches, etc. (Agliardia et al., 2001; Kinakin and Stead, 2005). Inherited tectonic faults are assumed to have a strong control on gravitational deformation of massifs (Scavia, 1995; Kaneko et al., 1997). Progressive failure within a rock slope can initiate and propagate in zones preferentially weakened by faults (Sartori et al., 2003; Bachmann et al., 2004; Willenberg, 2004). This seems to be the case in a well-documented area in the Argentera–Mercantour massif (Southern French Alps) where recent research revealed evidence linking pre-existing major tectonic fault zones and gravitational slope deformation (Guglielmi et al., 2005; Jomard et al., 2007a,b). This work however obtained few data on fault geometry at depth. The work focused on the characterisation of families of fault affecting hillsides subjected to gravitational failure (Follacci, 1987; Follacci, 1999; Guglielmi et al., 2002; Guglielmi et al., 2005; Jomard et al., 2007a, b). There is still a poor knowledge regarding the influence of fault geometry at depth on both in terms of the mobilized volume, and the kinematics of sliding associated with the gravitational failure.

We study the influence of complex fault zones and fault set geometry on massif-scale gravitational failure. This is undertaken by using a scaled physical modelling approach (Chemenda et al., 2005). This approach allowed examination of large-scale deformation, so that the initiation and propagation can be studied in the same experiment. Furthermore, this approach has no limitation on the introduction of different kinds of heterogeneities, such as fractures/faults (Sartori et al., 2003; Bachmann et al., 2004).

In order to analyse how the major fault network geometry at depth can influence both the failure propagation and global massif deformation, five sets of experiments were carried out. In the first, we considered a homogeneous model without faults. Second, we added six sub-vertical normal listric faults with an inflexion at shallow depth. Third, we increased the depth of the inflexion of the

* Corresponding author. Tel.: +33 492 94 26 20; fax: +33 492 94 26 10.
E-mail address: bois@geoazur.unice.fr (T. Bois).

0012-821X/$ – see front matter © 2008 Elsevier B.V. All rights reserved.
doi:10.1016/j.epsl.2008.06.006

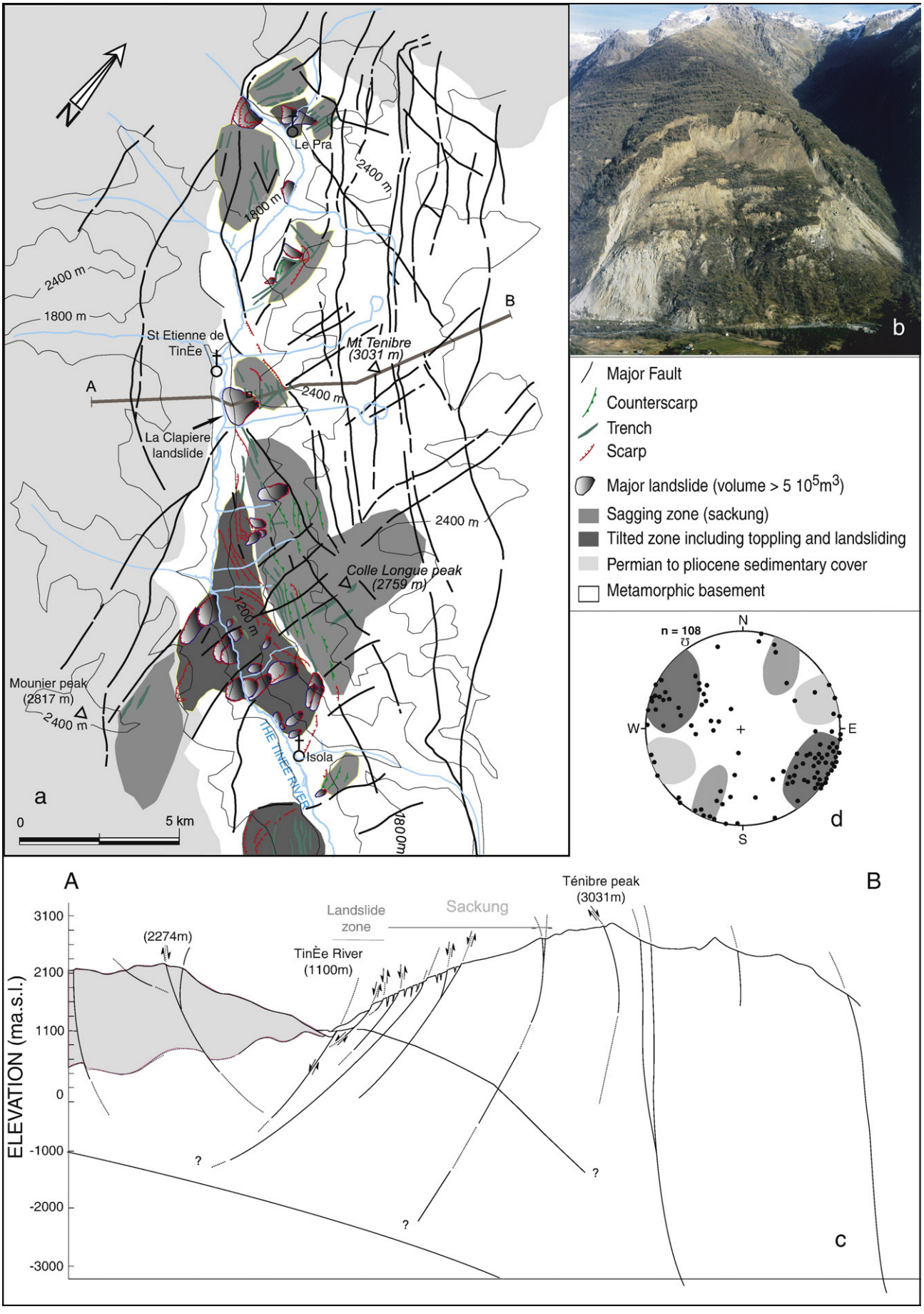
Le Pra
2400 m
1800 m
2400 m
1800 m
St Etienne de TinÈe
Mt Tenibre (3031 m)
A
B
2400 m
La Clapiere landslide
2400 m
Colle Longue peak (2759 m)
1200 m
Mounier peak (2817 m)
2400 m
THE TINEE RIVER
Isola
1800m
a
0
5 km
b
Major Fault
Counterscarp
Trench
Scarp
Major landslide (volume > 5 10^{5}m^3)
Sagging zone (sackung)
Tilted zone including toppling and landsliding
Permian to pliocene sedimentary cover
Metamorphic basement
n = 108
N
W
E
S
d
A
B
Ténibre peak (3031m)
Landslide zone
Sackung
(2274m)
TinÈe River (1100m)
ELEVATION (ma.s.l.)
3100
2100
1100
0
-1000
-2000
-3000
?
?
?
c

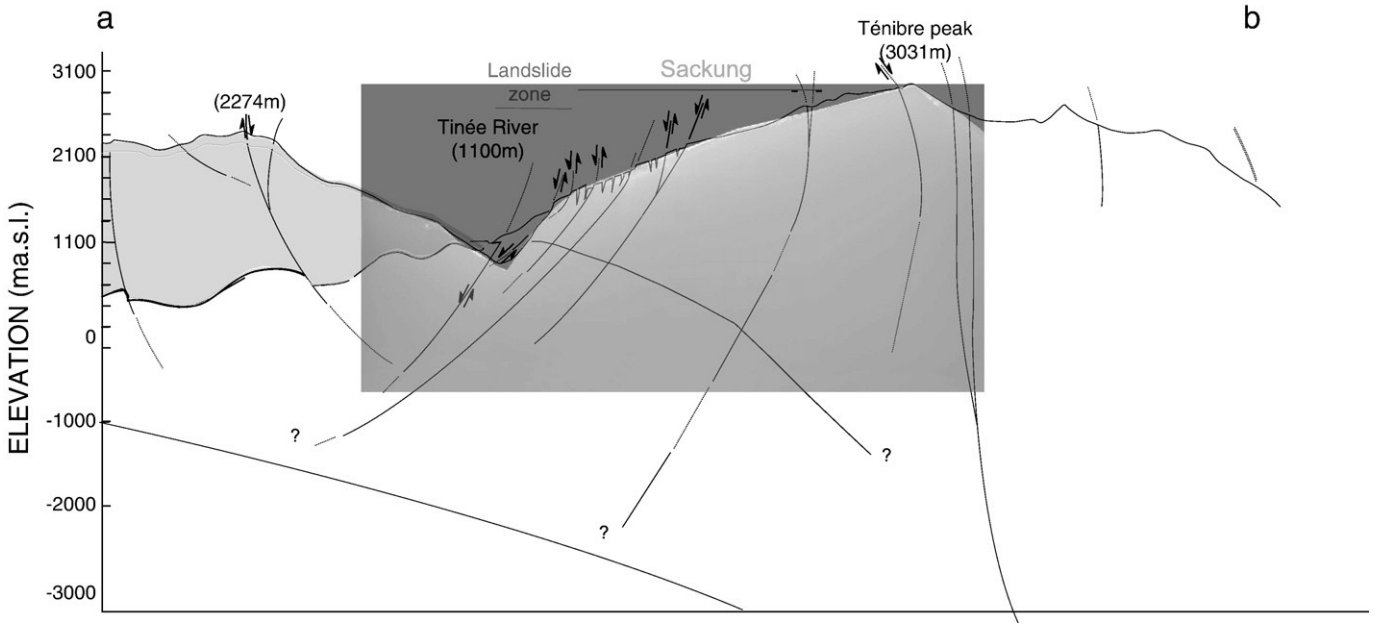

Fig. 2. Projection of the physical model boundaries at the field geological cross section.

normal listric faults. The fourth and fifth sets of experiments corresponded to the second and third, but with a thrust fault added at the slope toe.

2. Field data

The Tinée valley is situated along the North-Western edge of the Argentera–Mercantour metamorphic unit (Southern French Alps) (Follacci, 1999). The East side of the valley is mainly made of weathered metamorphic units that composed the metamorphic basement. This metamorphic basement has a N150–60°E foliation (average trend) (Bogdanoff, 1986).

Three distinct sets of faults affecting the valley can be distinguished, trending N010°E–N030°E, N080°E–N090°E and N110°E–N140°E (Ivaldi et al., 1991; Gunzburger and Laumonier, 2002; Delteil et al., 2003). Those pre-existing fault zones were mapped at the valley scale (Jomard et al., 2007a,b). Those faults display a pluri-kilometric lateral extension and a local thickness of several meters to tens of meters. Two groups of those faults can be distinguished. A set of normal faults that cut the entire slope from the foot to the crest with a dip towards the valley of 90° to 70°, and a single over-thrusting fault located at the foot of the slope in the Tinée valley floor with a dip of 20 to 30° towards the massif (Gunzburger et Laumonier, 2002; Jomard et al., 2006; Jomard et al., 2007a,b).

Several different gravitational features affect the valley slopes. They can roughly be grouped into two main types. The first type corresponds to a tilted zone, which is located near the foot of the slope between the elevation of the valley floor and the middle of the slope. The second is a sagging zone that is located between the mid-slope elevation and the mountain crest (Guglielmi et al., 2005; Lebourg et al., 2005) (Fig. 1).

In the tilted zone, metamorphic rocks are toppled by landslides. Volumes range between 5 and $50 \cdot 10^6$ m^3. Most of the currently active large landslides are located in this zone, and among them is the La Clapière (Fig. 1) which is less than 1 km downstream from the village of Saint-Etienne-de-Tinée. The behaviour of this landslide is typical of rock mass movements in the area. This landslide extends over a width of 800 m from foot of the hillside to a 120 m high scarp (at elevation 1600 m). The depth of the failure surface ranges from 100 m to 200 m. The landslide moves downward at a rate varying from 50 to 500 cm/yr, (with an average about 1 cm/day) (Casson et al., 2005; Jomard et al., 2006; Jomard et al., 2007a,b).

The sagging zone is characterized by extensional deformation structures (e.g. large pluri-kilometric length tension cracks and downhill scarps that are several meters high) (Lebourg et al., 2005). These landforms involve displacements along the pre-existing tectonic fault zones. Tension cracks correspond to a meter-wide horizontal opening of the superficial part of the faults that has created a 10 to 50 m deep normal trench (Guglielmi et al., 2005). Scarps correspond to shear displacements with vertical throws ranging from 1 to 50 m.

3. Experimental setup and procedure

A full description of the analogue material called *Slope*1 and of the loading device developed to perform scaled physical modelling of gravitational deformation is provided in (Chemenda et al., 2005). To create a model, the melted analogue material *Slope*1 is moulded into a rigid box. Faults are created by using strings stretched through openings (6 sub-vertical and 1 sub-horizontal) on the two opposing sides of the box. After cooling at a temperature of 20 °C, the material is strong enough to be easily cut with the strings without being damaged in areas other than the cuts. Strings are moved inside the openings to generate the faults and then removed. The main similarity criterion is:

$$\frac{\sigma_c^o}{\rho^o g^o H^o} = \frac{\sigma_c^m}{\rho^m g^m H^m} \quad (1)$$

where ρ g *is* the specific weight (ρ is the density and g is the gravity acceleration), σ_c the 7 strength under uniaxial compression, H the spatial scale of the phenomenon (the mountain 8 height H, for example) and superscripts “o” and “m” mean original and model, respectively. The scaling factor $\frac{H^o}{H^m}$ was chosen to be 1/50,000, so that 1 cm in the model corresponds to 10 500 m in nature (Fig. 2). Experiments were carried out at a fixed temperature of 20 °C. In this

Fig. 1. The Argentera–Mercantour massif and its deformation. (a) Plan view showing geology, fault and gravitational structures in the Argentera–Mercantour massif; (b) La Clapière landslide; (c) cross section AB on Figure 1a; (d) fracture orientations in the La Clapière landslide after Gunzburger and Laumonier (2002), modified.

condition *Slope*1 exhibits a high softening with $\sigma_c^m = 2500$ (Chemenda et al., 2005). This mechanical behaviour is 13 comparable to strength degradation behaviour introduced in some numerical models 14 (Hajiabdolmajid and Kaiser, 2002; Lebourg et al., 2003). At this temperature the coefficient of friction measured on the pre-existing fractures is $\mu = 0.2$.

The vertical faults have been numbered from F_1 near the valley toe, to F_6 near the crest. Then the model surface was shaped to the desired topography. The length of the model is thus equal to 14 centimeter and the width (third dimension) is equal to 30 cm. The third dimension has been chosen large enough to prevent any edge effects.

The model is then loaded in a vertical accelerator device. The latter consists in a mobile platform that can be uplifted up to 2 m and then released. During free fall the platform reaches a maximum velocity of 6 m s^{-1}. It is then decelerated to zero velocity on a shock absorber. The model undergoes strong acceleration (up to 500 m s^{-2}, during this phase) acting in the same direction as the gravity. Such an acceleration cycle is repeated several tens of time (usually 100 cycles). Model deformation can be observed accurately after each acceleration cycle. This discrete loading technique has proved to be equivalent to a continuous quasi-static loading (Chemenda et al., 2005). Cross-sections were made at the end of each experiment by cutting the model at various locations after cooling it to 10 °C.

The mobilized volume has been determined in each case by calculating the unstable surface multiplied by 1. Then the result was converted in cubic meters using the scaling factor.

4. Results

Each experiment was performed at least 5 times in order to ensure the validity of the result. Only the most representative results are presented below.

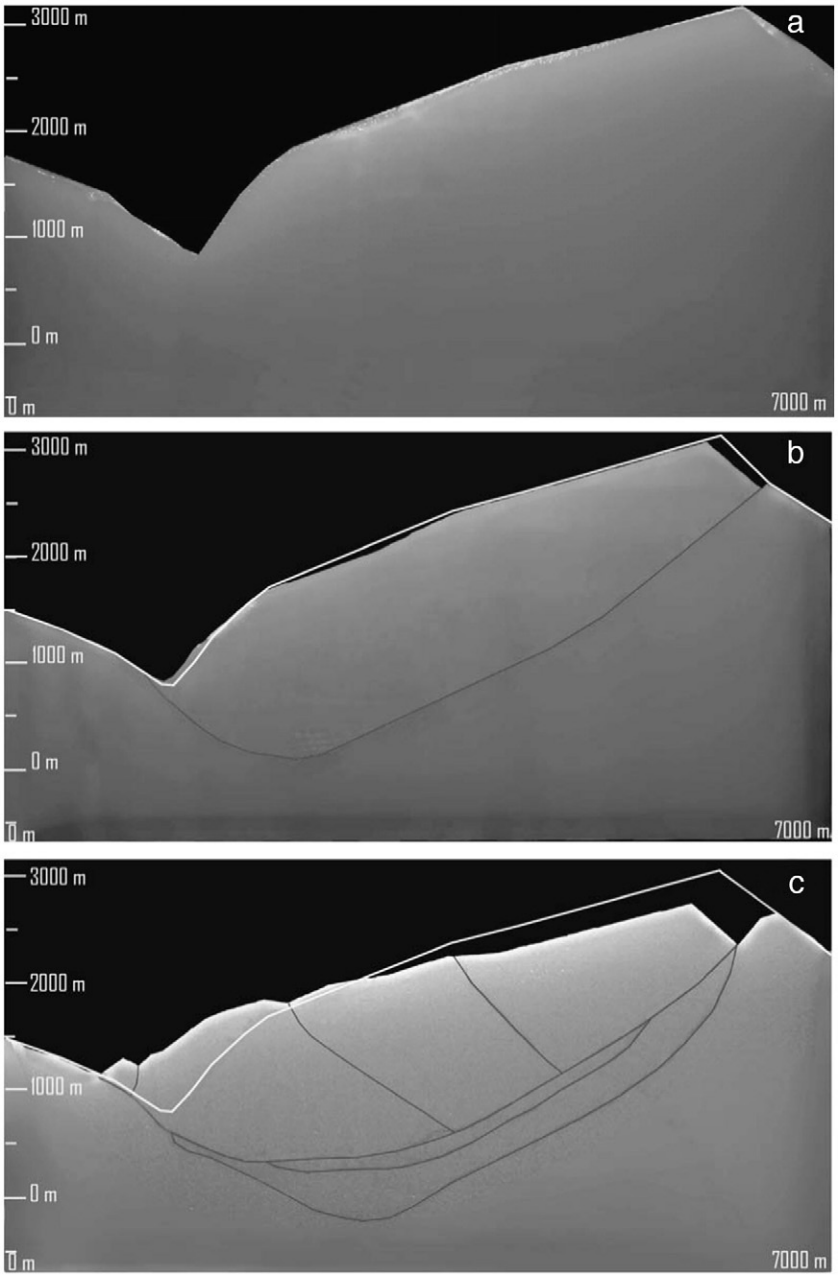

Fig. 3. Case 1, the homogeneous model. (a) The initial non-deformed model; (b) the first deformation stage; (c) the last deformation stage.

4.1. Progressive failure analysis

4.1.1. Case 1: Homogeneous model

A model without any faults is first considered (Fig. 3a). On the initial deformation stage (Fig. 3b), a master fault formed in the model at a maximum depth of about 1500 m and bound a large unstable volume. A 100 m high scarp formed behind the topographic crest. In the final stage of deformation, the master fault delimitating the sliding unit developed a complex fracture network (fault zone) that became wider when the displacement of the sliding unit increased (Fig. 3c). Failure reached a maximum depth of 2200 m. Two faults perpendicular to the master fault zone were observed. The previously formed escarpment kept growing and reached 400 m in height.

4.1.2. Case 2: A slope cut by 6 normal listric faults with an inflexion at "shallow" depth

In this case, 6 normal listric faults with an inflexion at the same elevation than the 4 valley floor (about 1000 m) are added to the homogeneous model (Fig. 4a). In the initial 5 deformation stage (Fig. 4b), superficial non-elastic deformation occurred on three inherited 6 normal faults and on a newly formed gravitational fault. On the inherited fault close to the 7 topographic crest (F_6) an escarpment of 100 m in height formed. On the inherited faults close 8 to the toe (F_2 and F_3) two normal trenches can be observed. Finally, a new formed 9 gravitational fault formed at the toe of the slope and propagated inside the massif as a sub-horizontal thrust fault. Internal irreversible deformation took place along this thrust fault but also along an antithetic normal fault initiating from the inflexion

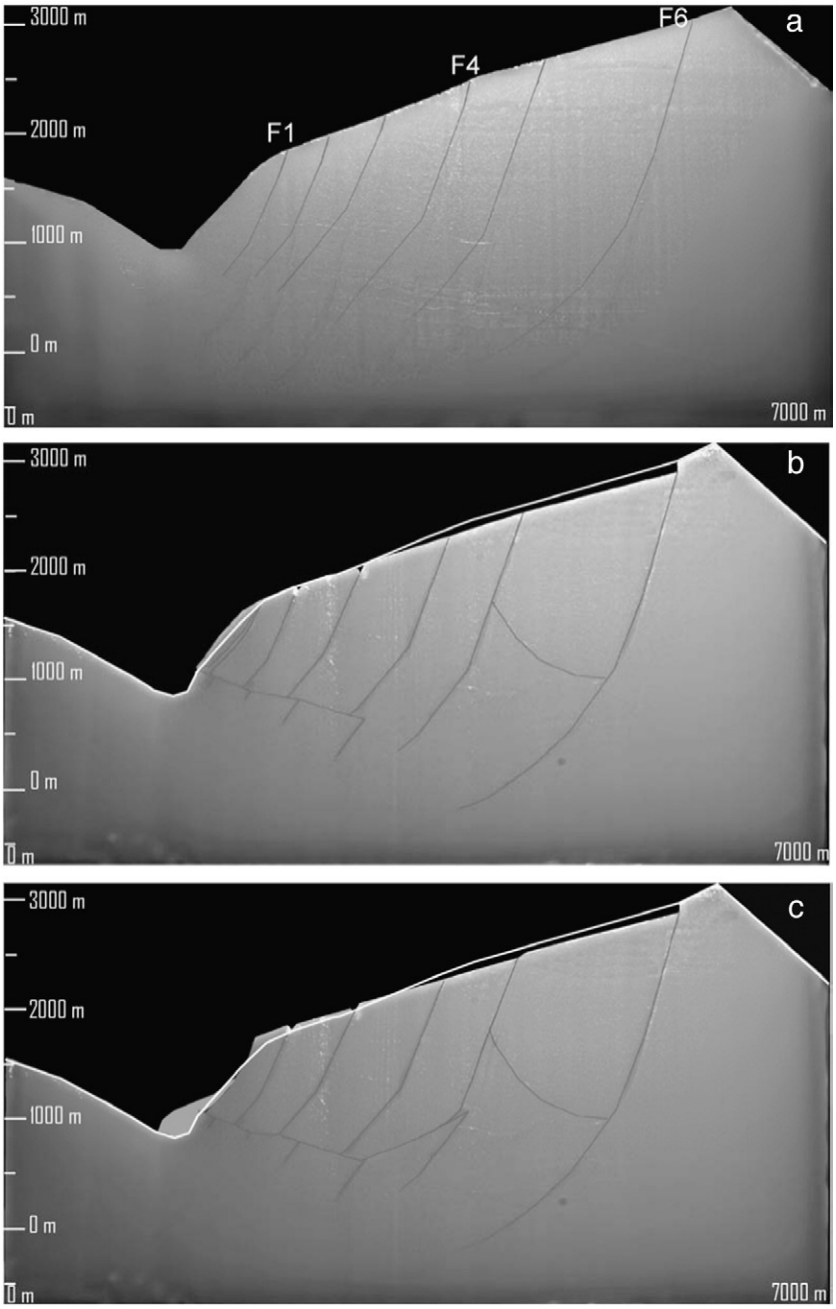

Fig. 4. Case 2, slope cut by 6 normal listric faults with an inflexion at "shallow" depth. (a) The initial non-deformed model, (b) the first deformation stage; (c) the last deformation stage.

point of fault F_6 and propagating towards the topographic surface (Fig. 4c). This gravitational normal fault and inherited fault F_6 delineate a large block of about $20 \cdot 10^6 +/- 2 \cdot 10^6$ m^3 that is moved downslope. In the final stage of deformation the newly formed thrust fault had propagated through the connection of inflexion points of the faults F_4 to F_6, delineating a deep-seated gravitational moving zone. A relatively small superficial landslide of about $10 \cdot 10^5 +/- 2 \cdot 10^5$ m^3 occurred between the first normal fault and the slope toe.

4.1.3. Case 3: A slope cut by 6 normal listric faults with an inflexion at depth

In this configuration the inflexion of the faults is about 1000 m deeper than in the case (Fig. 5a). In the initial deformation stage, superficial non-elastic deformation was mainly localized on the normal fault F_6, near the topographic crest (Fig. 5b). Internal deformation produced on a fault initiating from fault F_6 at a depth of 1700 m below the surface. The dip of this newly formed fault was oriented toward the valley. At the final deformation stage (Fig. 5c), this had fault propagated to the toe of the slope to form a deep fault zone delineating a mobilized volume. A persistent antithetic fault also formed and propagated from the lower part of fault F_6 towards the topographic surface producing a toppling on faults F_1 and F_2.

4.1.4. Case 4: A slope cut by 6 normal listric faults with an inflexion at shallow depth and with a thrust fault

In this case, a pre-existing thrust fault is added to the configuration tested in case 2 (Fig. 6a). In the initial deformation stage, all the pre-existing faults were activated and accommodated most of the non-elastic deformation (Fig. 6b). Four scarps appeared on faults F_2, F_3, F_4 and F_6, respectively with scarp heights of 100, 100, 160 and

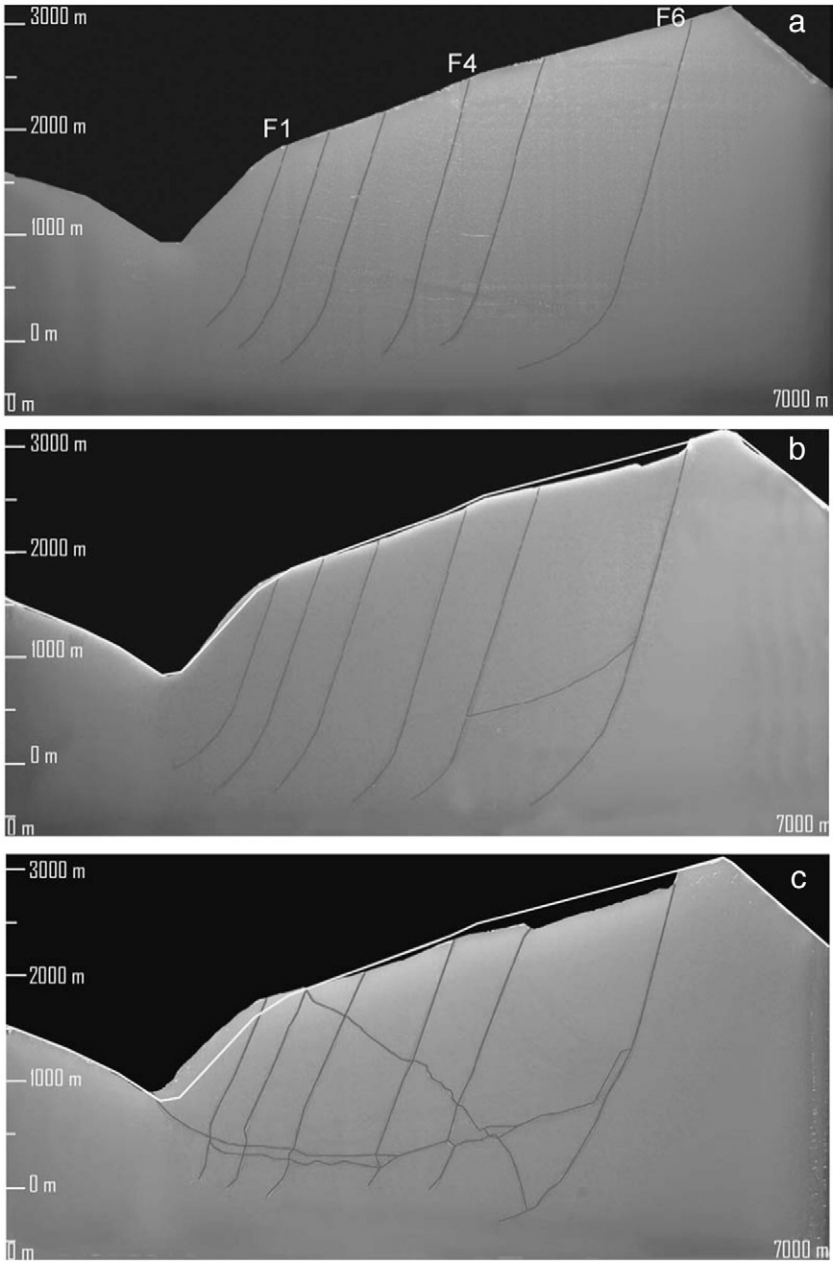

Fig. 5. Case 3, slope cut by 6 normal listric faults with an inflexion at depth. (a) The initial non-deformed model; (b) the first deformation stage; (c) the last deformation stage.

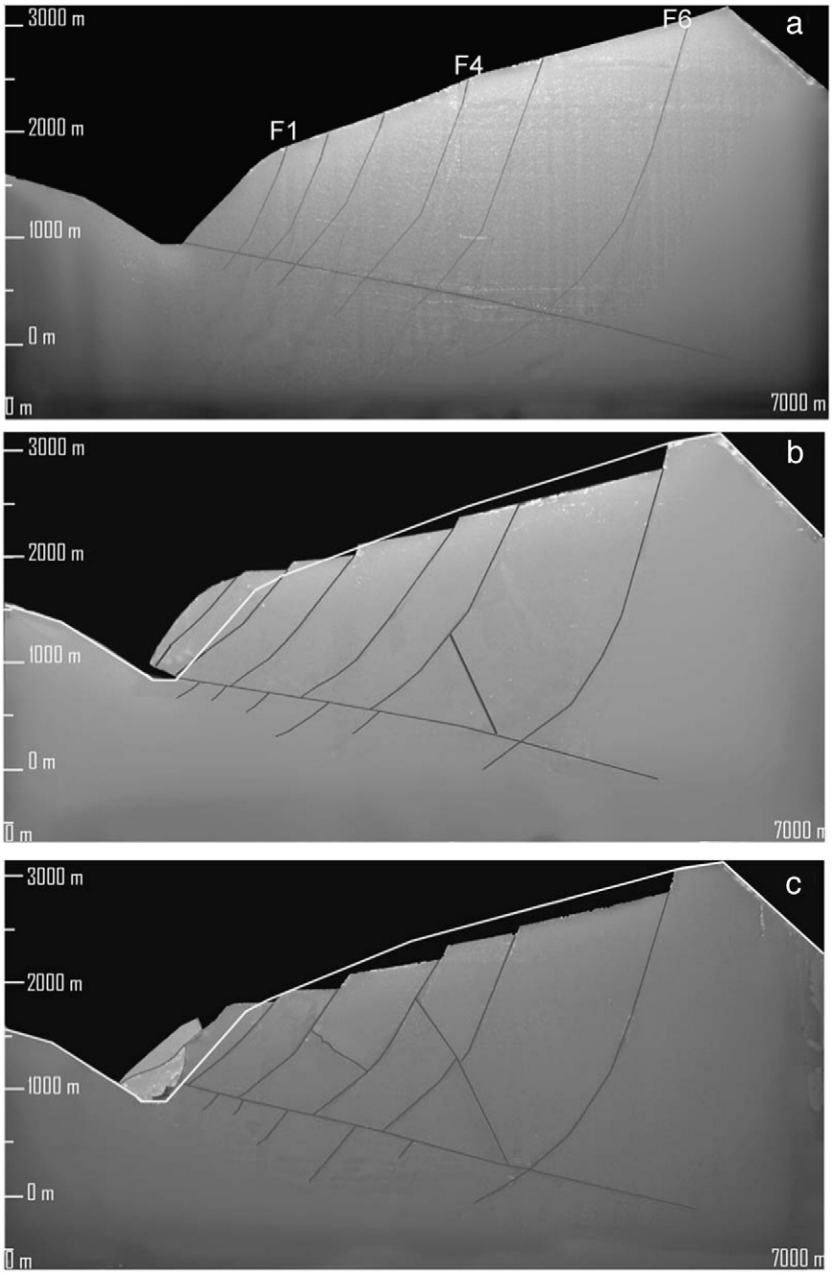

Fig. 6. Case 4, slope cut by 6 normal listric faults with an inflexion at shallow depth and a thrust fault. (a) The initial non-deformed model; (b) the first deformation stage; (c) the last deformation stage.

270 m. The mobilized volume, bounded by the thrust fault at depth and the normal fault F_6, moves along the thrust fault producing sliding on blocks bounded by the normal faults and the thrust fault. At the final deformation stage, antithetic normal faults had propagated through the blocks. The block bounded by the first normal fault, the thrust fault, and the valley was activated as a large landslide with an estimated volume of about $25 \cdot 10^5 + / - 2 \cdot 10^5$ m^3 (Fig. 6c).

4.1.5. Case 5: A slope cut by 6 normal listric faults with an inflexion at depth and a thrust fault

In this case, a pre-existing thrust fault is added to the configuration tested in case 3 (Fig. 7a). In the initial deformation stage, the deformation was mainly localized on fault F_6F6 producing a 100 m in height escarpment, and on the thrust fault (Fig. 7b).The mobilized volume moved along the thrust fault producing the toppling of the sub-vertical faults near the valley. At the final deformation stage, a normal fault had appeared behind the topographic crest and had propagated toward the basal thrust fault (Fig. 7c). This normal fault was sub-vertical close to the topographic surface and it dip 45° at depth. Secondary superficial antithetic normal faults propagated and formed counterscarps near the topographic surface all along the moving mass. A V-shaped structure appeared below the thrust fault.

4.2. Displacement analysis

Both vertical and horizontal displacements were measured on the surface and at depth by comparing cross-sections between initial configuration and the final stage of deformation. This was undertaken by comparing the position of selected points, which were easily identifiable (e.g. the topographic crest, the trace of

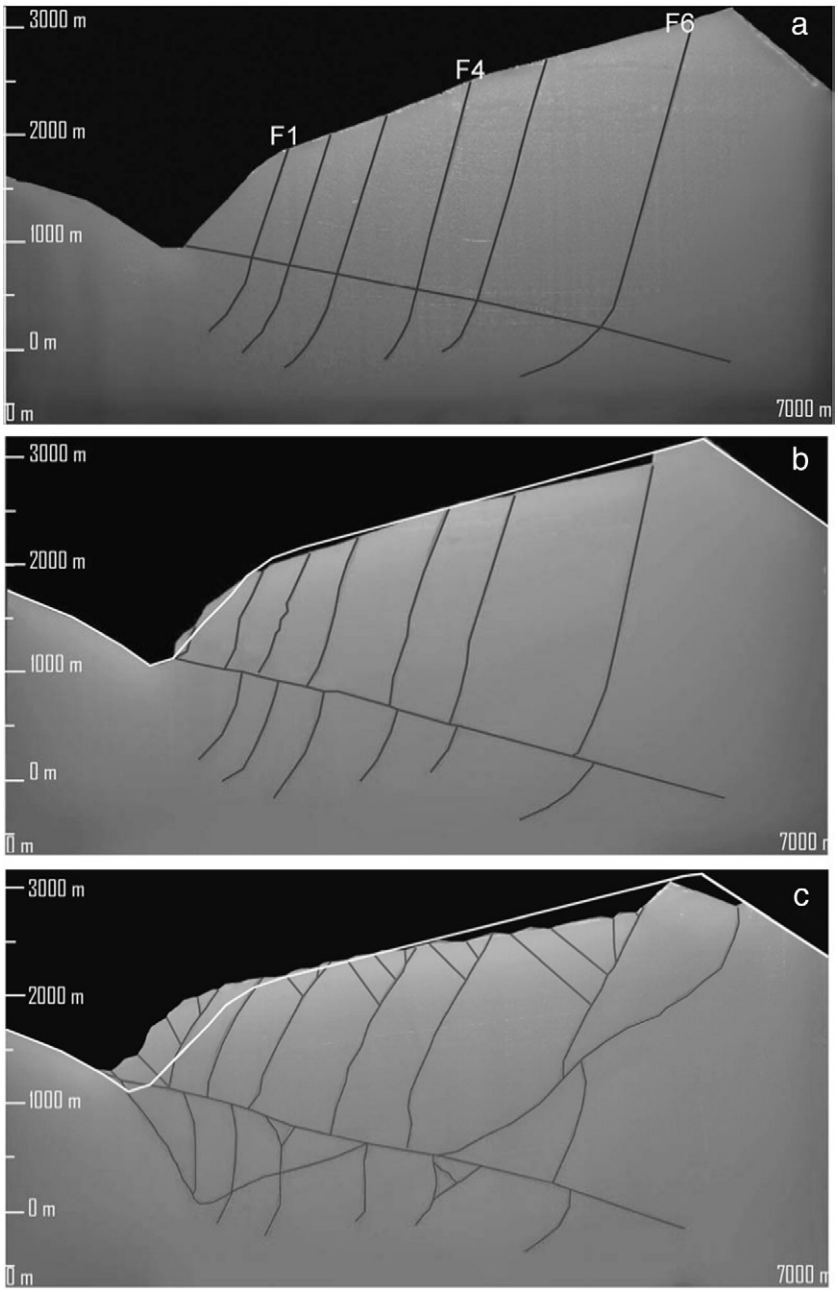

Fig. 7. Case 5, slope cut by 6 normal listric faults with deep inflexion and thrust fault. (a) The initial non-deformed model; (b) the first deformation stage; (c) the last deformation stage.

faults on the topographic surface, the inflexion point of faults at depth). The horizontal component (Ux) of the displacement vector was considered positive for displacement from the right to the left of the model, whereas the vertical component (Uz) of displacement was considered positive for displacement from the bottom to the top of the model. The magnitude of the displacements (Di) was normalized using Eq. (2), to compare the different cases studied.

$$\mathrm{Di} = \frac{U_i}{Ui_{\max} - Ui_{\min}} \tag{2}$$

Where i can be equal to x or z.

These displacements are plotted against their position relative to the valley ($L/L\max = 0$ form the point located on the valley and $L/L\max = 1$ form the point located on the crest). D_x and D_z are only reported in cases 2 and 4 (Fig. 8). The three cases without a pre-existing thrust fault (e.g. cases 1, 2 and 3), and the two cases with a pre-existing thrust fault (e.g. cases 4 and 5) were directly comparable.

For cases without a pre-existing thrust fault (cases 1, 2 and 3) at the surface (Fig. 8a and b), the displacements are localized on the topographic crest and at the valley wall. On the crest, both D_x and D_z are localized on fault F_6 or on a newly formed fault behind the crest. D_x is positive (Fig. 8a) while D_z is negative (Fig. 8b). Near the valley, D_x is still positive but a strong change is observed between F_2 and F_1 and between F_1F1 and the valley wall (Fig. 8a). D_z becomes positive between F_2 and F_1 (Fig. 8b). This is compatible with a rising of the valley bottom. At depth, below the topographic crest, D_x is positive (Fig. 8c) while D_z is negative (Fig. 8d). In the middle part of the model, faults F_5 to F_1 are much more activate than at the topographic surface. Both D_x and D_z have positive values on faults F_5 to F_1. Below the valley, both D_x and Dz are positive, but their value decreases from F_1 to the bottom of the valley. This

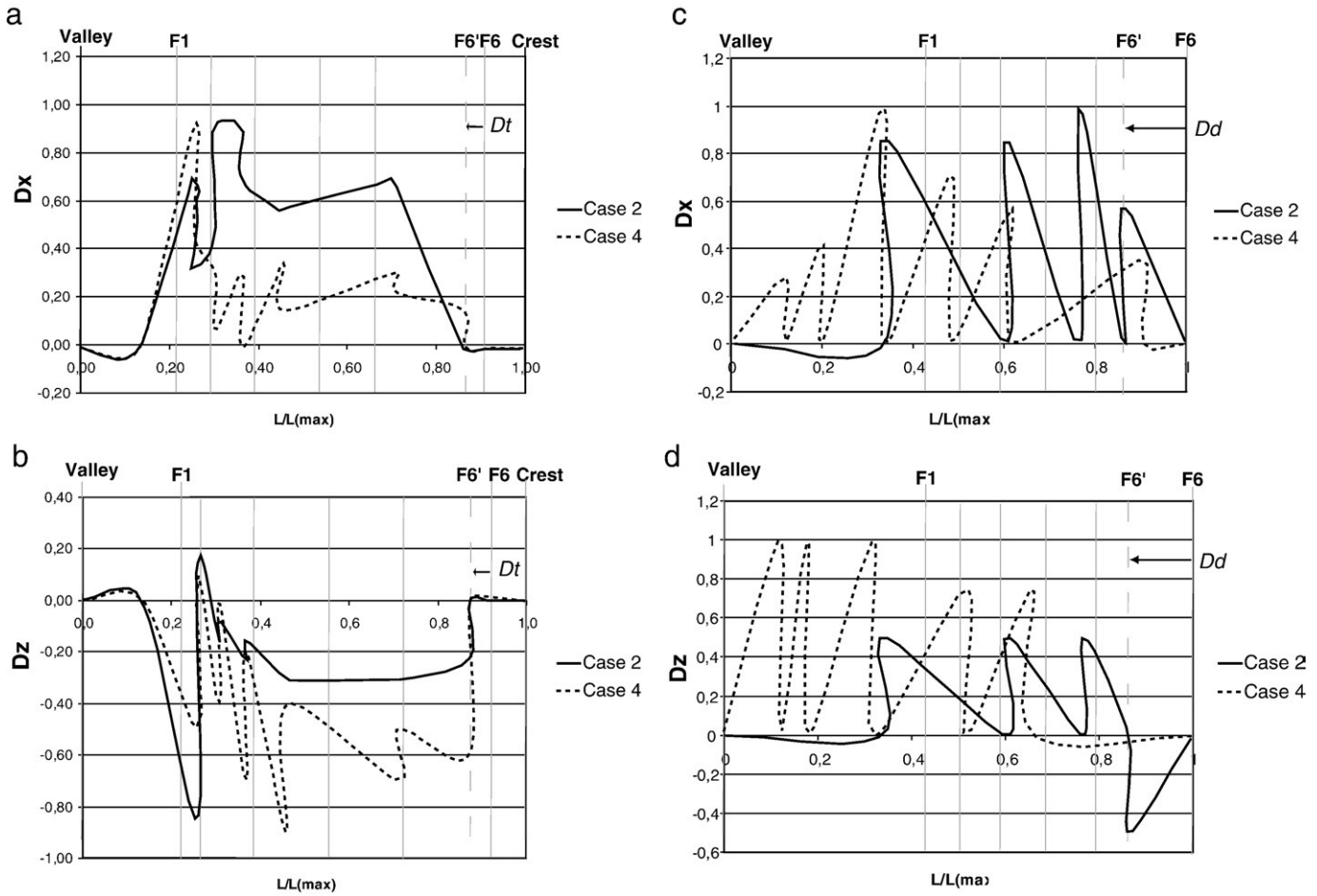

Fig. 8. Horizontal and vertical displacements of the topographic surface and at depth at the final deformation step. a) Horizontal displacements at the topographic surface; b) vertical displacements at the topographic surface; c) horizontal displacements at depth; d) vertical displacements at depth. The vertical grey lines correspond to the initial position of the pre-existing normal faults. D_tDt corresponds to the total horizontal displacement between the initial position of the fault F_6, and its final position represented by F_6'. D_d corresponds to the total vertical displacement between the initial position of the fault F_6, and its final position represented by F_6'.

displacement pattern at the surface and at depth (depression of the topographic crest and rising of the valley), seems to indicate that, in cases 1, 2 and 3 the mobilized mass had a strong global rotational component.

For cases 4 and 5 (with a pre-existing thrust fault), displacement pattern different from cases 1–3 was observed. At the topographic surface from the topographic crest to the valley, faults F_1 to F_6 have a positive horizontal (D_x) and a negative vertical displacement (Dz). At depth, from below the crest to the bottom of the valley, both D_x and Dz are once again distributed across faults. The displacement pattern indicated that the mobilized mass corresponded to translational movement along the pre-existing thrust fault followed by activation of the six pre-existing normal faults.

Globally, regardless of the initial configuration of the model, the displacement is much more intense at depth than at the surface.

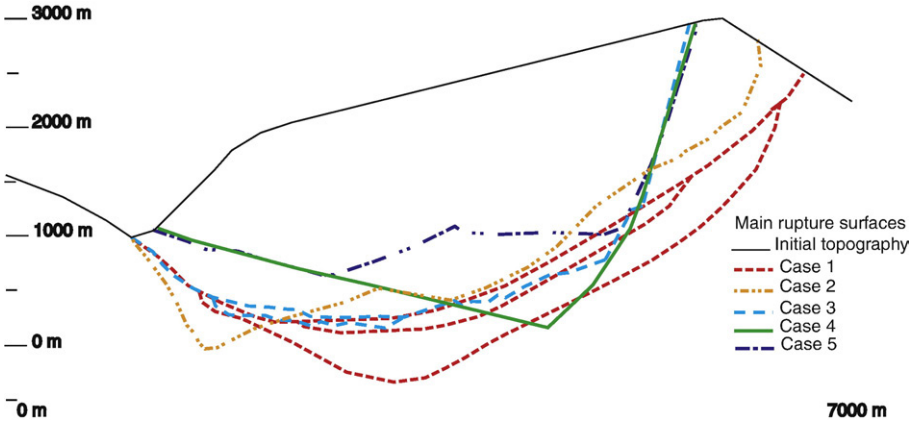

Fig. 9. Main failures obtained for all tested configurations.

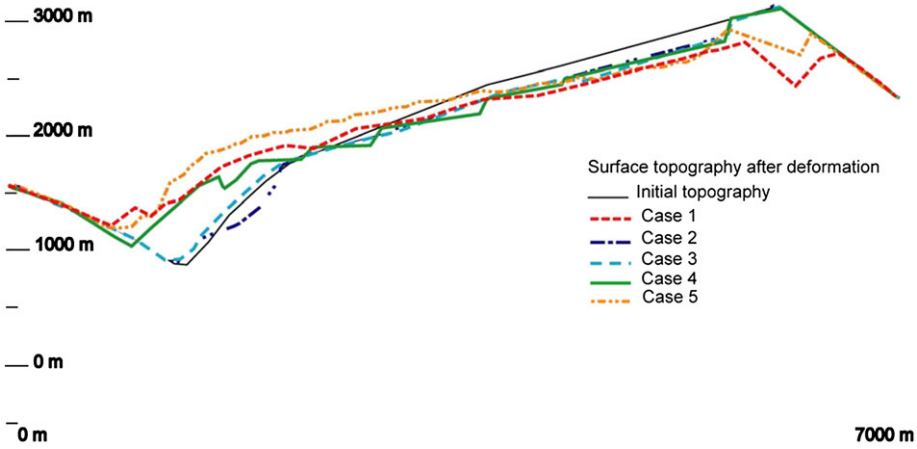

Fig. 10. Final deformed topographies for each case.

Indeed the displacement at surface (D_t) is always lower than the displacement at depth (D_d) (Fig. 8a to d).

5. Discussion

Our models provide new insight on the influence of inherited faults on gravitational induced deformation, linking surface deformation to deep-seated failures.

5.1. Comparison between models and the Argentera–Mercantour massif

There are many similarities between the models and the example of the La Clapière landslide. The case 2 configuration (Fig. 4), however, displays the best fit to the field deformation observed at the landslide. Similarities between case 2 model and observed field deformation include the following:

i Normal fault scarps, comparable to those observable on the natural slope, were formed on faults F_5 and F_6
ii Trenches on normal faults, comparable to those observable on the natural slope, were formed on faults F_2F2 and F_3.
iii Counterscarps connecting the topographic surface and faults F_4 to F_6 formed.
iv A Deep-Seated Landslide, comparable with the La Clapière landslide, formed at the toe of the slope.
v A thrust fault comparable with the one observed at the toe of the La Clapière slope formed. This point allows us to propose that this thrust fault has been tectonically formed during alpine orogenesis and then sealed (Ivaldi et al., 1991; Lebourg et al., 2005). Due to gravitational deformation, a part of this thrust fault has probably been reactivated to accommodate the currently active large landslide.
vi The displacement pattern resulting from the model cases without pre-existing thrust fault was in good agreement with results obtained from multi-temporal remote sensing images analyses of La Clapière hillside (Casson et al., 2005). In this study it has been shown that the overall movement of the La Clapière hillside tends to be rotational rather than translational.

Moreover, for each tested configuration, the deformation at the mountain scale can be characterized by the formation at depth of a major fault zone, more or less curved and complex, on which the entire unstable mass slides. Average unstable mass volume ranges between $78 \cdot 10^9$ and $49 \cdot 10^9$ m^3 m^3 +/− $3 \cdot 10^9$ depending on the case. In the La Clapière area, this kind of structure is not clearly identified, but the mountain scale collapse is suggested by recent studies (Jomard et al., 2006; Jomard et al., 2007a,b; Bachmann et al., 2006).

5.2. Sensitivity of rock slope gravitational deformation to large pre-existing fault

Results showed that the pre-existing faults and their geometries have a strong control on the massif gravitational deformation pattern.

First, the addition of a sub-horizontal thrust fault leads to a complete modification of the displacement pattern of the unstable mass (from rotational to translational). The latter affects also the location of the main failure surface, but has little influence on the mobilized volume (Fig. 9).

Second, the depth of the inflexion of the pre-existing normal faults has a strong control on surface deformation (Fig. 10). Deep inflexion of the normal listric faults produces very little superficial deformation. Conversely shallow inflexion produces normal trenches on the surface.

Each of the 5 cases tested has shown that, regardless the initial configuration of pre-existing faults, a Deep-Seated Gravitational Deformation and a more superficial slope deformation (e.g. toppling of the hillside or small-scale landslide) occurs. This is in good agreement with other natural examples for which pre-existing faults are favorably oriented with strikes along the slope (e.g. the Deep-Seated Gravitational Slope deformation of Rosone, Piemont, Italy (Barla and Chiriotti, 1995), or the Séchilienne landslide near the city of Grenoble, France (Guglielmi et al., 2002)). Our results indicate that the complexity of gravitational deformation on the surface can give insight regarding the presence and orientation of pre-existing fractures within a hillside. Deformations can often be difficult to observe on natural examples because of a lack of good exposures.

To our knowledge, many field studies neither carefully analyze surface deformation nor faults geometries at depth. However, these steps are of critical importance in determining hazard and possible mitigation options. Indeed, depending on the geometry of pre-existing faults, gravitational deformation can result in a simple Deep-Seated Gravitational Slope Deformation or in a slow deep-seated gravitational movement with superficial or potentially catastrophic landslides.

6. Conclusion

Our work indicates that the presence, orientation, and continuity of pre-existing fractures in a hillside likely control the style of gravitational deformation. The geometry of the normal listric faults at depth has a strong control on the deformation of the topographic surface but no real influence on the depth of the main sliding plane or on the total mobilized volume. Indeed the addition of a thrust fault completely modified the displacement pattern of the unstable mass for a modelled hillside in the Southern French Alps.

The different deformations of the topographic surface obtained in each of the 5 cases that we tested were a function of the geometry of the listric faults—in particular the depth of the inflexion point. An inflexion point located at shallow depth results in a sliding dynamic of the hillside, whereas deeper inflexion points leads to the toppling of the hillside. These relatively small-scale movements (sliding or toppling of the hillside) are consequences of a deeper movement involving not only the hillside but the entire massif (Bachmann et al., 2006; Agliardi et al., 2001; Bachmann et al., 2008). The depth and the mobilized volume of the deformation of the massif were function of the geometry of the fault network, so we conclude that pre-existing fault geometry is of critical importance determining not only the fault networks affecting a massif, but also the geometries of new faults formed by gravitational deformation. Moreover any study of slope destabilization must take into account not only the hillside affected by the movement, but also the entire massif.

To confirm these results and test the influence of the topography on the slope stability, 3-D physical models will be developed.

Acknowledgments

We sincerely thank J. Coe and another anonymous reviewer for the constructive suggestions, criticisms and improving the English.

This work has been supported by the G.I.S C.U.R.A.R.E research program.

References

Agliardia, F., Crosta, G., Zanchib, A., 2001. Structural constraints on deep-seated slope deformation kinematics. Eng. Geol. 59, 83–102.

Bachmann, D., Bouissou, S., Chemenda, A., 2004. Influence of weathering and pre-existing large scale fractures on gravitational slope failure: insights from 3-D physical modelling. Natural Hazards and Earth System Sciences, vol. 4, pp. 711–717.

Bachmann, D., Bouissou, S., Chemenda, A., 2006. Influence of large scale topography on gravitational rock mass movements: new insights from physical modeling. Geophys. Res. Lett. 33, L21406, doi:10.1029/2006GL028028.

Bachmann, D., Bouissou, S., Chemenda, A., 2008. Analysis of massif fracturing during Deep Seated Gravitational Slope Deformation by physical and numerical modelling. Geomorphology, doi:10.1016/j.geomorph.2007.09.018.

Barla, G., Chiriotti, E., 1995. Insights into behaviour of the large deep seated gravitational slope deformation of Rosone, in the Piemont Region (Italy). Felsbau 13, 425–432.

Bogdanoff, S., 1986. Evolution de la partie occidentale du massif cristallin externe de l'Argentera. Place dans l'arc alpin: Géologie de la France 4, 433–453.

Casson, B., Delacourt, C., Allemand, P., 2005. Contribution of multi-temporal remote sensing images to characterize landslide slip surface — application to the La Clapière landslide (France). Natural Hazards and Earth System Sciences, vol. 5, pp. 425–437.

Chemenda, A., Bouissou, S., Bachmann, D., 2005. 3-D Physical Modeling of Deep-Seated Landslides: new technique and first results. J. Geophys. Res. 110, F04004, doi:10.1029/2004JF000264.

Crosta, G.B., 1996. Landslide, spreading, deep-seated gravitational deformation: analysis, examples, problems and proposals. Geogr. Fis. Din. Quat. 19, 297–313.

Delteil, J., Stéphan, J.F., Attal, M., 2003. Control of Permian and Triassic faults on Alpine basement deformation in the Argentera massif (external southern French Alps). Bull. de la Société Géologique de France 174, 481–498.

Follacci, J.P., 1987. Les mouvements du versant de la Clapière à Saint-Etienne-de-Tinée (Alpes-Maritimes). Bull. Lab. Ponts et Chaussées 150–151, 107–109.

Follacci, J.P., 1999. Seize ans de surveillance du glissement de terrain de La Clapière (Alpes-Maritimes, France). Bull. Lab. Ponts et Chaussées 220, 35–51.

Guglielmi, Y., Vengeon, J.M., Bertrand, C., Mudry, J., Follacci, J.P., Giraud, A., 2002. Hydrogeochemistry: an investigation tool to evaluate infiltration into large moving rock masses (case study of La Clapière and Séchilienne alpine landslides. BullEng. Geol. Environ. 61 (4), 311–324.

Guglielmi, Y., Cappa, F., Binet, S., 2005. Coupling between hydrogeology and deformation of mountainous rock slopes: insights from La Clapière area (southern Alps, France). C. R. Geosci. 337, 1154–1163.

Gunzburger, Y., Laumonier, B., 2002. Origine tectonique du pli supportant le glissement de terrain de la Clapière (Nord-Ouest du massif de l'Argentera - Mercantour, Alpes du Sud, France) d'après l'analyse de la fracturation. C.R. Geosci. 334, 415–422.

Hajiabdolmajid, V., Kaiser, P.K., 2002. Slope stability assessment in strain-sensitive rocks. EUROCK 2002, Proceedings of the ISRM International Symposium on Rock Engineering for Mountainous Regions, Funchal, Madeira, pp. 237–244.

Ivaldi, J.P., Guardia, P., Follacci, J.P., Terramorsi, S., 1991. Plis de couverture en echelon et failles de second ordres associés à un décrochement dextre de socle sur le bord nord-ouest de l'Argenterra (Alpes-Maritimes, France), C.R. Acad. Sci. Paris 313, 316–368 serie II.

Jomard, H., Lebourg, T., Tric, E., 2007a. Identification of the gravitational discontinuity in weathered gneiss by geophysical survey: La Clapiere landslide (France). Appl. Geophys. J. Appl. Geophys. 62, 47–57.

Jomard, H., Lebourg, T., Binet, S., Tric, E., Hernandez, M., 2007b. Characterisation of an internal slope movement structure by hydro geophysical surveying. Terra Nova 19, 48–57.

Kaneko, K., Otani, K.J., Noguchi, Y., Togashiki, N., 1997. Rock fracture mechanics analysis of slope failure. In: Asaoka, A., Adachi, T., Oka, F. (Eds.), Deformation and Progressive Failure in Geomechanics. Elsevier, New York, pp. 671–676.

Kinakin, D., Stead, D., 2005. Analysis of the distribution of stress in natural ridge forms: implications for the deformation mechanisms of rock slopes and the formation of sackung. Geomorphology 65, 85–100.

Lebourg, T., Riss, J., Fabre, R., Clément, B., 2003. Morphological characteristics of till formations in relation with mechanical parameters. Math. Geol. 35, 835–852.

Lebourg, T., Binet, S., Tric, E., Jomard, H., El Bedoui, S., 2005. Geophysical survey to estimate the 3D sliding surface and the 4D evolution of the water pressure on part of a Deep Seated Landslide. Terra Nova 17, 399–406.

Sartori, M., Baillifard, F., Jaboyedoff, M., Rouiller, J.D., 2003. Kinematics of the 1991 Randa rockslides (Valais, Switzerland). Natural Hazard and Earth System Sciences, vol. 3, pp. 423–433.

Scavia, C., 1995. A method for the study of crack propagation in rock structures. Geothechnique 45, 447–463.

Tibaldi, A., Rovida, A., Corazzato, C., 2004. A giant deep-seated slope deformation in the Italian Alps studied by paleoseismological and morphometric techniques. Geomorphology 58, 27–47.

Willenberg H., Geologic and Kinematic model of a complex landslide in crystalline rock (Randa, Switzerland), *Ph.D Thesis*, Swiss Federal Institute of Technology, Zurich (2004), 161 pp.